Research Article | Vol. 27, No. 9 | 29 Apr 2019 | OPTICS EXPRESS 12183
Optics EXPRESS

Balanced-detection interferometric cavity-assisted photothermal spectroscopy

JOHANNES P. WACLAWEK,* CHRISTIAN KRISTAMENT, HARALD MOSER, AND BERNHARD LENDL

Research Unit of Environmental Analytics, Process Analytics and Sensors, TU Wien, Getreidemarkt 9/164, 1060 Vienna, Austria
**johannes.waclawek@tuwien.ac.at*

Abstract: An optical cavity can be utilized as an excellent transducer for highly sensitive gas detection with the application of photothermal spectroscopy, featuring the beneficial property of an ultra-low absorption volume within a rugged sensing element. We report the novel implementation of balanced detection in Fabry-Perot photothermal interferometry via two identical 1 mm-spaced cavities. That way, excess noise limiting the sensitivity of previous cavity-based photothermal sensors was effectively rejected close to the fundamental limit of shot noise. A quantum cascade laser served as mid-infrared excitation source to induce refractive index changes in the sample, and a near-infrared fiber laser served as probe source to monitor the photo-induced variations. The metrological qualities of the sensor were investigated by SO_2 detection. For the targeted absorption band centered at 1380.93 cm^{-1}, a 5 ppbv minimum detection limit was achieved with a 1 s integration time, corresponding to a normalized noise equivalent absorption of 7.5×10^{-9} cm^{-1} W $Hz^{-1/2}$. Additionally, the sensor showed excellent long-term stability, enabling integration times of a few thousand seconds.

1. Introduction

The spectroscopic analysis of gaseous species down to trace concentration levels is of importance across a variety of fields, including environmental monitoring, industrial process control, medical diagnostics, and scientific research [1–4]. Any absorption of electromagnetic waves by molecules excites their internal energy levels, which in turn may lead to sample heating via energy transfer due to collisional relaxation. A photo-induced temperature change within the excited sample volume is directly proportional to the concentration and absorption coefficient of the absorbing molecule as well as to the incident laser power, and inversely proportional to the modulation frequency and cross-section of the laser beam [5]. A change in the sample's temperature causes in turn a change in density and pressure. Changes in the sample's thermodynamic properties are used for trace detection in photothermal spectroscopy (PTS) and photoacoustic spectroscopy (PAS), which probe, respectively, changes in the refractive index and acoustic waves [5,6]. These methods are classified as indirect absorption measurements techniques, and they offer unique features including a large dynamic range over a few orders of magnitude and ideally being background-free. PTS methods, which employ an interferometer as a sensitive transducer for monitoring the photo-induced changes in the sample's properties, are powerful instruments for detection of trace gases [7–14]. Typically, these photothermal interferometry (PTI) setups employ an excitation laser for transient sample heating and a probe laser to monitor the resulting refractive index changes. Any change in the refractive index causes a phase shift of the electromagnetic waves passing through the heated region, which can easily be measured by detection of the probe laser's intensity transmitted through the interferometer. Both, two-beam interferometers, such as the Mach-Zehnder [7–9] or Jamin [10] type, and multi-beam interferometers, such as the Fabry-

#346419 https://doi.org/10.1364/OE.27.012183
© 2019 Received 20 Sep 2018; revised 29 Mar 2019; accepted 30 Mar 2019; published 17 Apr 2019

Optics EXPRESS

Perot configuration [11–14], i.e., an optical cavity, have been applied to measure temperature-induced phase shifts of laser radiation.

The use of an optical cavity as a transducer with PTI offers the unique characteristic that the transmission is a function of both the induced phase shift and the reflectivity of the cavity mirrors. A very simple configuration thus enables the possibility of designing highly sensitive transducers with ultra-short interferometer spacing through the application of moderately to highly reflective mirrors. Any enhancement in sensitivity due to an increase in the mirrors' reflectivity, however, is directly proportional only to the point at which the source of limiting noise is not also proportionally enhanced. Limiting noise may be introduced via excess noise of the probe laser source, such as frequency and intensity noise, as well as environmental noise. Moreover, the generated photothermal signal is directly proportional to the induced temperature change, which in turn is inversely proportional to the laser beam cross-section area [5]. Hence, for a given laser power, induced temperature changes are higher in smaller excitation volumes, making a Fabry-Perot interferometer with short spacing an ideal candidate for sensor miniaturization even down to a sample volume of a few mm^3. Although the miniaturization of high sensitivity gas sensors is of great interest for various applications, the potential of a compact Fabry-Perot-PTI sensor has only been rudimentarily shown thus far, i.e., in [13,14]. In addition to the advantage of a small footprint, a low sample volume entails a fast sensor response time. A drawback of the basic Fabry-Perot-PTI scheme proposed in [11–14], however, is that it suffers from increased noise levels caused by excess noise, severely limiting the sensitivity and ruggedness of the sensor. Due to the use of an interferometer consisting of an optical cavity as the transducer for detection of the photo-thermally induced refractive index changes, and the spectroscopic purpose of the excitation laser, we subsequently refer to PTI using an optical cavity as *interferometric cavity-assisted photothermal spectroscopy* (ICAPS).

Excess laser noise can be efficiently removed in the signal path by application of balanced detection [15]. The beam is split into two equal parts by means of a beam splitter and detected by two separate photo-diodes. Differential amplification of the two detector signals allows rejection of the common mode noise, i.e., noise that is present in both paths. In a basic balanced-detection absorption spectroscopy setup, both beams ideally carry the same excess noise. If both photo-diodes detect the same intensity in the absence of any absorbing species, the two signals cancel each other and a zero differential output voltage, limited by fundamental shot noise, is detected [16,17]. However, if one beam is affected by any absorption, then the balance of the photocurrents is disturbed, yielding a differential output voltage. In contrast to an optical cavity, the sensitivity of a two-beam interferometer configuration (e.g., Mach-Zehnder type) is only dependent on the phase shift, resulting in a limited potential for miniaturization of highly sensitive devices. However, this type of interferometer inherently enables improvement of the sensor's sensitivity by rejection of common mode noise by application of balanced detection using the two complementary output branches [10]. Such a balanced-detection scheme will not only enhance the sensitivity of a given PTI setup but also increase the ruggedness of the sensor due to enhanced immunity to external disturbances.

This work reports for the first time on the metrological principle of balanced-detection ICAPS via application of two Fabry-Perot interferometers with identical characteristics. This scheme links the general advantages of the optical cavity transducer of the PTI method with the advantages arising from the use of balanced detection and its shot noise limited detection. Balanced detection was realized with only two interferometer mirrors. Within these two mirrors, two Fabry-Perot interferometers were established by simultaneous transmission of two equal parts of the probe laser with lateral displacement. The same sample gas was thus present in both cavities. When applying balanced detection, identical characteristics of the two cavities, which also includes uniform sample properties, such as sample composition, pressure, and temperature inside the transducers, are essential in order to adjust the

Optics EXPRESS

transmission modes of both interferometers to identical frequencies, which is a requirement for effective simultaneous noise subtraction. This is of particularly high relevance for real-world applications, where rapid changes may occur in the target molecule and/or matrix. Effective noise cancelation was enabled by a feedback control, which ensured identical positioning of the transmission modes in terms of frequency and thus identical transmitted noise intensities of the two beams, resulting in auto-balancing of the scheme. High sensitivity was accomplished by employing a cavity with moderate finesse and small spacing together with strong photo-thermal signal generation by application of high excitation laser intensities. Refractive index changes induced by the excitation laser were monitored by a sample probe laser intersecting the excitation beam in the transverse direction, due to favorable properties such as very simple beam alignment and avoidance of heating the interferometer mirrors, which could alter the optical path length of the cavity. By this means, a simple, robust, and compact gas sensor design with no moving parts was enabled. The transient generation of the photothermal signals was performed by applying wavelength modulation (WM) at reduced sample pressure via a powerful continuous wave (CW) distributed feedback (DFB) quantum cascade laser (QCL) as excitation source. Strong fundamental absorption features of the sample molecules in the mid-infrared (mid-IR) region could thus be targeted. The photo-induced transducer signal was detected within a narrow bandwidth by a lock-in amplifier (LIA) at the second harmonic (2*f*) of the modulation frequency [18]. This scheme is a powerful method for increasing the signal-to-noise ratio as well as the selectivity of a given measurement. Refractive index changes were detected via a CW-DFB fiber laser (FL) emitting in the vicinity of 1550 nm together with a photodiode. This near-infrared region offers mature technology, and high-performing optical components are readily available. The metrological qualities of this 2*f*-WM balanced-detection ICAPS principle were investigated using sulfur dioxide (SO_2) as the target molecule.

2. Basic sensor operation principle, balanced detection, and system architecture

2.1. Basic sensor operation principle

Changes in the refractive index of a sample are primarily caused by changes in its density. Usually, density decreases with increasing temperature; thus, the refractive index decreases by heating the sample. In the case of small temperature variations induced by the photothermal effect, the sample's refractive index change is directly proportional to the induced temperature change [5]. A change in the refractive index of a gaseous sample can be detected with high sensitivity by monitoring the phase shift of electromagnetic radiation passing through a Fabry-Perot interferometer (FPI). Such a device consists of two partially reflecting parallel mirrors separated by a certain distance. The transmitted intensity I_T through an ideal FPI is given by [19]

$$I_T = I_0 \frac{1}{1+\left(\frac{2F}{\pi}\right)^2 \sin^2\left(\frac{\Delta\varphi}{2}\right)}, \tag{1}$$

where I_0 is the incident intensity, F is the finesse of the optical cavity, and $\Delta\varphi$ is the phase difference. The finesse in turn is determined by the reflectivity R of the two interferometer mirrors:

$$F = \pi \frac{\sqrt{R}}{1-R}, \tag{2}$$

and the phase difference for a cavity round trip, i. e., twice the distance d of the spacing of the mirrors of the FPI, is given by

Optics EXPRESS

$$\Delta\varphi = \frac{2\pi}{\lambda_0} 2nd\cos\theta, \tag{3}$$

where λ_0 is the vacuum wavelength, n is the refractive index, and $\cos\theta$ is the angle of incidence. Therefore, a variation of n causes a variation of $\Delta\varphi$, which causes a variation of the transmitted intensity through the FPI incorporating the sample at a certain frequency. The ICAPS operation principle is illustrated in Fig. 1; the periodic transmission function [Eq. (1)] of the interferometer is shifted with respect to the vacuum wavelength when the refractive index of the sample in between the two mirrors changes due to photothermal heating. This shift is monitored as a change in the transmitted intensity by a photodiode, using a probe laser that is tuned to a frequency enabling partial transmission through the interferometer. The greatest sensitivity to variations in the phase difference is found near the inflection point on one side of the periodic transmission function, which is at approximately 75% transmission. At this point, the slope of the function is at its maximum and is roughly linear over a narrow range, yielding a linear sensor response to induced temperature changes. The slope of the periodic transmission function and therefore the strength of the detectable photo-induced signal is by approximation proportional to the finesse of the cavity, which is only dependent on the reflectivity of the mirrors. By this means, the sensor's sensitivity can be adjusted by adjusting the finesse of the employed cavity.

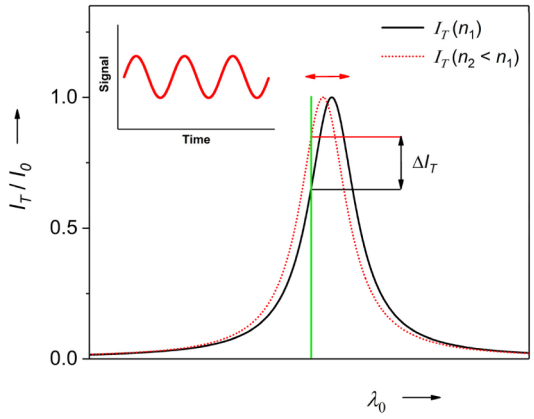

Fig. 1. ICAPS operation principle; the frequency of a probe laser (green line) is tuned to near the inflection point of the periodic transmission function of the cavity, which incorporates sample gas at thermal equilibrium (black trace). Photo-induced heating of the sample by an excitation laser decreases the refractive index of the gas, which is accompanied by a shift in the transmission function with respect to the vacuum wavelength (red dotted trace). This shift is monitored via a change in the transmitted probe laser intensity (ΔI_T) detected using a photodiode. The inset shows the monitored signal for periodic sample heating.

2.2. Balanced-detection ICAPS

Considering a constant signal strength, the signal-to-noise ratios of ICAPS setups [10–14] are limited by elevated noise content comprising excess probe laser noise and environmental noise. Excess probe laser noise arises from frequency and intensity fluctuations of the emitted radiation whose characteristics depend on the used laser type. Environmental noise may be introduced by acoustic and mechanical perturbations, which may induce on the one hand variations in the refractive index of the media inside the cavity due to pressure changes and on the other hand tiny variations in the cavity geometry, both of which affect the transmission function characteristics. Any noise is ultimately detected by the photodiode as intensity fluctuations. Both sources of noise can be minimized to some extent, respectively, by using a narrow linewidth laser source with low intensity noise characteristics and by employing an

Optics EXPRESS

adequate sensor enclosure. Nevertheless, the noise cannot be removed completely by these means. The system's excess noise, however, can be eliminated down to the fundamental limit of shot noise in an elegant way by application of a balanced-detection scheme using an additional probe laser reference path [15,16]. The probe laser's intensity is simultaneously compared with and without the absorption signal, allowing effective rejection of common mode noise. The concept of balanced-detection ICAPS (BICAPS) is schematically depicted in Fig. 2; the probe beam is split by a beam splitter into two equal beams – a sample probe beam and a reference probe beam. Both beams are transmitted through the same interferometer mirrors and the same sample gas with some lateral displacement. By this means, each beam is transmitted through a separate cavity – a sample cavity and a reference cavity – with identical characteristics. However, only the sample probe beam intersects with the excitation beam, thus propagating through the photo-induced heated region of the target molecules experiencing refractive index variations caused by the thermal wave. Hence, the detected signal of the sample probe beam carries the photothermal signal, which is superimposed by noise originating from various sources. In contrast, the reference probe beam only probes noise due to the lateral displacement of the excitation beam in combination with the strong damping of a thermal wave. Both beams are detected by separate photodiodes, whose signals are subtracted. Identical noise present in both parts is thus canceled with a high rejection ratio. The fundamental limit of this noise reduction scheme is imposed by shot noise. The application of balanced detection greatly enhances the signal-to-noise ratio of the presented sensor by enabling the recovery of tiny photothermal signals. Moreover, the ruggedness and compactness of this sensing scheme are improved due to enhanced impassivity to environmental noise, leading to more relaxed enclosure requirements. In contrast to the strong photothermal signal probed by the sample probe beam, the reference probe beam may also probe a weak photoacoustic signal, which propagates in the media only slightly damped, insignificantly effecting the total detected signal proportionally within the two interferometers.

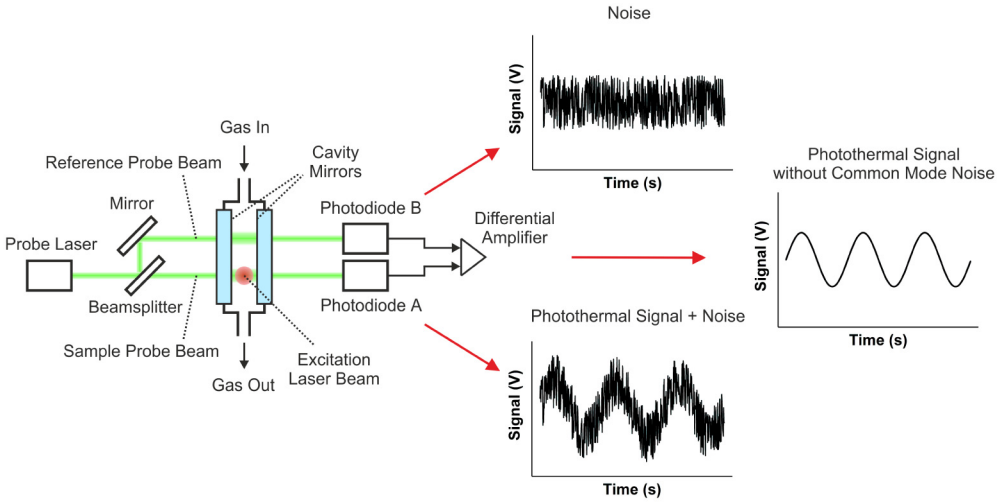

Fig. 2. Balanced-detection ICAPS scheme; the probe beam is split into a sample probe beam and a reference probe beam. The sample beam probes the photothermal signal, which is superimposed by noise, whereas the reference beam only probes noise. By differential amplification of the two photodiode signals, the photothermal signal is recorded along with effective rejection of common mode noise.

A key feature of the implementation of balanced detection in the ICAPS sensor principle is that this scheme allows the sensitivity to be increased via an increase in the cavity finesse

Optics EXPRESS

without a simultaneous increase in noise. This arises because noise that is enhanced proportionally to the finesse is afterwards canceled by the balanced-detection scheme.

2.3. Sensor architecture

The architecture of the 2*f*-WM balanced-detection ICAPS based gas sensor is schematically depicted in Fig. 3. The optical cavities used as the transducer for monitoring induced changes in the refractive index were build up within a single air-spaced etalon, which consisted of two 30 mm diameter fused silica plates at which dielectric-coated mirrors with reflectivity of $R = 0.985$ were deposited. Spacers of 1 mm thickness fixed these mirrors to each other. The real behavior of a plane FPI mirror configuration resulted in an effective finesse of approximately 89 of the applied FPIs instead of the theoretical finesse of 208 according to Eq. (3), which can be calculated for an ideal optical cavity. Photothermal-induced refractive index changes inside the sample cavity were monitored via a fiber-coupled, single-mode tunable CW-DFB-FL. The FL emitted a beam at a wavelength of ~1550 nm with a constant optical output power of 40 mW, and its wavelength could be thermally tuned within a total range of approximately 1.2 nm. The emitted fiber-coupled output beam was collimated by a fixed-focus aspheric lens collimator with a short focal length yielding a beam dimeter of roughly 0.9 mm and coupled into the cavities with a narrowed beam waist diameter and large Rayleigh length ($R_L \approx 100$ mm) by using a plano-convex CaF_2 lens ($f = 100$ mm), prior to splitting it by means of a beam splitter into sample and reference probe beams. Because the direction of propagation of the reference probe beam changes, an additional mirror was used to deflect the beam back to the initial propagation direction. By this means, the two parallel beams were transmitted through the two mirrors with a lateral displacement of ~10 mm. The intensities of the individually transmitted beams were detected by two photodetectors consisting of a gallium indium arsenide (GaInAs) positive intrinsic negative junction (PIN) photodiode together with a transimpedance amplifier (TIA). Because the physical dimensions of the two photodetectors required a lateral beam displacement larger than 10 mm, the two beams were additionally deflected by two mirrors after transmission through the photothermal cell. Each beam was again collimated by a plano-convex lens (collimation lenses are not sketched in Fig. 3 to aid clarity). Neutral density filters ensured to not saturate the detectors, whereby an optical power of ~1.9 mW was impinging on each detector. Finally, the outputs of the two photodiodes were passed to a low-noise differential amplifier, whose output was further fed to a lock-in amplifier (LIA). Selective heating of the sample gas inside the interferometer was performed by using a collimated CW-DFB-QCL emitting at a wavelength of 7.25 µm (excitation laser), which was housed in a high heat load (HHL) package. Here, frequency tuning could be performed by varying the QCL temperature via injection current and temperature control by a Peltier element, respectively. The QCL output beam was focused by a plano-convex CaF_2 lens ($f = 50$ mm), in between the two mirrors forming the sample cavity to induce strong photothermal excitation via the high laser intensity, intersecting the standing wave of the sample probe beam in the transverse direction only. Focusing of the QCL beam yielded a Gaussian beam waist diameter of about 140 µm. The combination of high excitation laser intensity and small beam waist of the probe laser beam ensured high sensitivity of the sensor. The sensor platform was based on photothermal sample excitation via WM and detection of the second harmonic (2*f*) by demodulation of the alternating current (AC) component of the differentially amplified photodetector signals, i.e., the balanced signal, using a LIA. Further data processing was carried out via a LabVIEW-based program after transferring the digitized data to a computer. After transmission through the measurement cell, the QCL beam was guided through a reference cell filled with SO_2 in N_2 at an absolute pressure of 133 mbar onto a thermo-electrically cooled mercury-cadmium-telluride (MCT) photodetector. The reference gas cell and the photodetector were used as the reference channel for tightly locking the QCL frequency to the center of the selected SO_2 absorption line using the 3*f* LIA output. The direct current (DC) injection current component

Optics EXPRESS

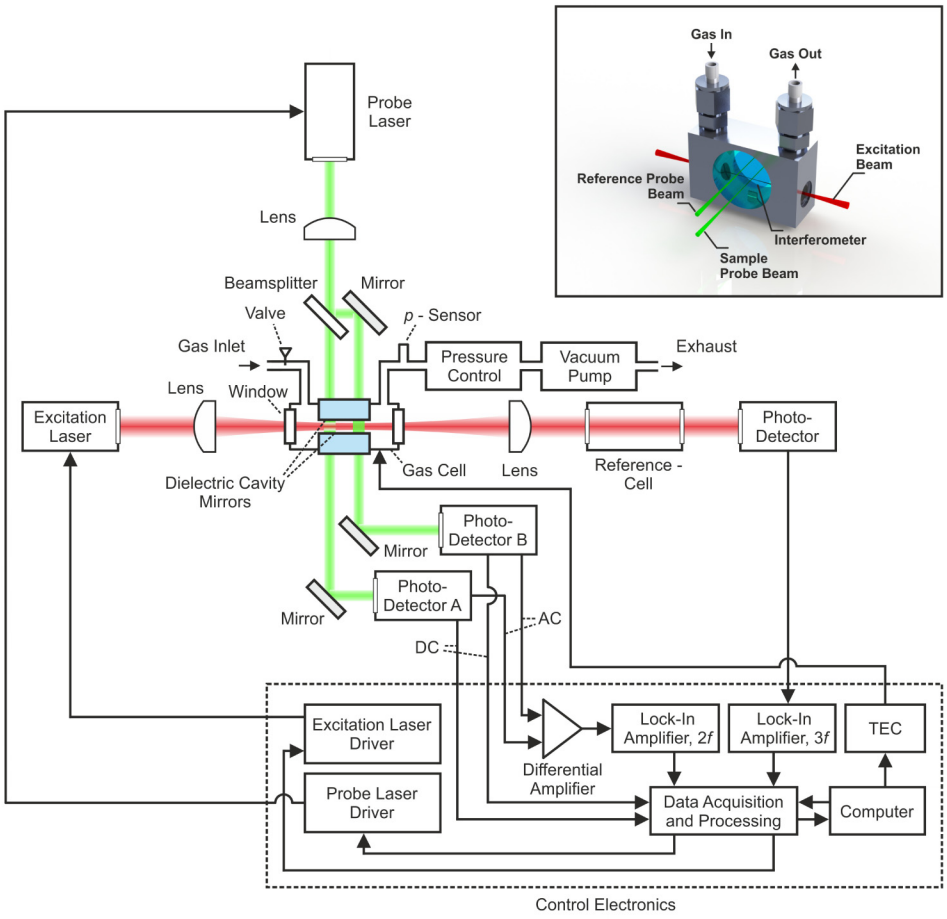

Fig. 3. Schematic of the ICAPS based gas sensor employing balanced detection. Inset: Illustration of the compact gas cell including the interferometers with a mirror spacing of 1 mm.

of the QCL was adjusted proportionally via electronic feedback control to maintain the emission at the desired frequency, preventing a long-term drift of the QCL frequency. The interferometer substrates were fixed into a compact and gastight aluminum cell, and transmission of the QCL beam through the cell was enabled by two CaF_2 windows. Sample gas exchange was via a gas in- and outlet. An illustration of the designed compact and gastight balanced-detection ICAPS cell is shown as an inset in Fig. 3. The outer dimensions of the cell were 55 × 35 × 21 mm with a total inner sample gas volume of <2 cm^3. The DC component of the photodetector, which monitored the transmitted sample probe beam intensity (photodetector A), was used to maintain the probe lasers' emission frequency at the inflection point of the sample cavities' transmission function via a slow feedback circuit (mHz). By this means any drift of the transducer, e.g., by temperature or changing sample gas composition, was automatically compensated. The inflection point of the reference interferometer was kept at the probe laser's emission frequency by monitoring the reference probe beam intensity through the reference cavity (photodetector B) and by controlling the temperature of the measurement cell, which allowed fine-adjustment of the interferometer spacing, again using a slow feedback circuit (mHz). By using two independent feedback circuits, the probe laser was locked to the inflection, while the transmission functions of the two cavities were locked to the same frequency. This yielded identical response to noise, thus

Optics EXPRESS

enabling efficient noise rejection. To implement the WM technique, the emission wavelength of the QCL was modulated by adding a sinusoidal function to the DC injection current input. Modulation of the probe laser intensity was induced when the temperature of the sample between the sample cavity was altered by absorption of the excitation laser by the target molecules. The ICAPS detection was performed in two different modes: scan and locked. In the scan mode, spectra of the sample gas were acquired by slowly tuning (mHz) the QCL frequency over the desired spectral range around the target absorption line through a change of the DC injection current component according to a sawtooth function. In the locked mode, the QCL frequency was locked to the center of the selected SO_2 absorption line, ensuring stable long-term measurements. The pressure and flow of the sample gas inside the measurement cell was controlled and maintained by using a metering valve, pressure sensor, pressure controller, and mini diaphragm vacuum pump. The metrological qualities of the presented sensor were investigated by employing a modulation frequency of f_{mod} = 297 Hz, a modulation depth of $\Delta\nu = \pm$ 0.09 cm^{-1}, a LIA time constant set to τ = 1 s, and a sawtooth excitation laser tuning frequency of f = 6.67 mHz. The absolute pressure and flow of the sample gas was kept constant at p = 200 mbar and u = 25 mL min^{-1}.

3. Experimental

3.1. Sulfur dioxide absorption band selection

To investigate the metrological qualities of the sensor, sulfur dioxide (SO_2) was used as the target molecule due to its strong and separated absorptions within the spectral region covered by the employed QCL. A simulated spectrum of the selected SO_2 absorption band (base-10) for photothermal excitation centered at 1380.93 cm^{-1} is shown in Fig. 4. This absorption band is situated within the ν_3 fundamental spectral range, which extends from 1400 to 1300 cm^{-1} (see inset Fig. 4).

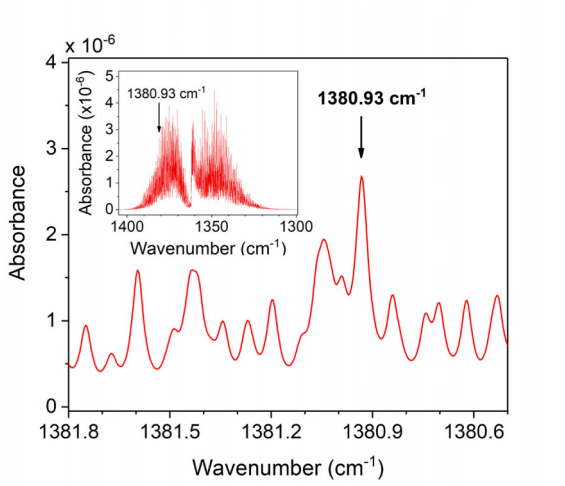

Fig. 4. HITRAN2016 simulated absorption spectrum (base-10) of 1 ppmv SO_2 (p = 200 mbar, l = 1 cm, T = 296 K) [20].

3.2. Selectivity, sensitivity, and linear response of the sensor

The balanced-detection ICAPS sensor's selective response to SO_2 traces was investigated by recording spectra for different concentrations of SO_2 in N_2 within the range from 0 to 1000 parts per billion by volume (ppbv) by tuning the QCL wavelength across the selected SO_2 absorption band centered at 1380.93 cm^{-1}. Different concentration levels were achieved by diluting a 1 ppmv SO_2 calibration mixture with N_2 using a custom gas mixing system.

Optics EXPRESS

Figure 5 shows the measured results for three different SO_2 concentration levels as well as the noise floor of the sensor for pure N_2.

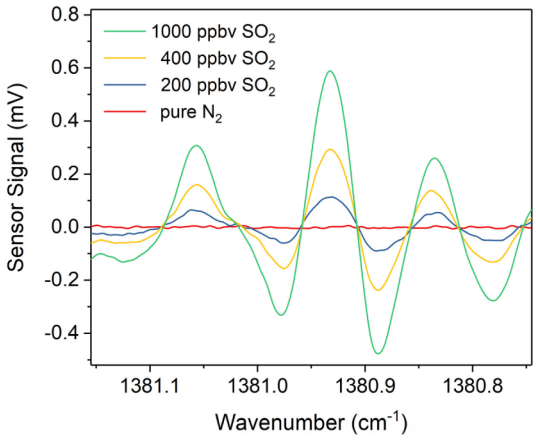

Fig. 5. 2*f*-WM balanced-detection ICAPS spectra of three different SO_2 concentrations together with the noise floor of the sensor for pure N_2 recorded at an absolute pressure of $p = 200$ mbar when the QCL frequency was tuned over the absorption band centered at 1380.93 cm^{-1}.

Investigation of the balanced-detection ICAPS sensor's sensitivity and linearity as a function of the SO_2 concentration was performed by continuous monitoring of different concentration levels within the range of 0 to 1000 ppbv by utilizing the locked mode at which the QCL frequency was fixed to the center of the selected SO_2 absorption line by means of the reference path. 2*f*-WM signals were acquired for a total duration of 10 min for each concentration level. The signal acquisition was stopped for 1 min when the SO_2 concentration was changed to allow the concentration to stabilize. The measurement results are shown in Fig. 6. This figure also shows a comparison of the sensor noise when the cell was flushed with pure N_2 for balanced and non-balanced detection and ICAPS. To aid clarity, an offset of 0.1 mV was added to the noise signal of the non-balanced detection. A comparison of the standard deviations of the recorded noise for the two different configurations showed that an improvement in sensitivity of 21.1 dB (factor 11.3) was achieved by application of the balanced-detection scheme. Averaging of the data for each concentration step yielded excellent linearity between the measured signal amplitudes and the SO_2 concentrations, as shown in the inset of Fig. 6. Based on the averaged signal amplitudes for 200 ppbv SO_2 and the standard deviation of the noise level for pure N_2, a signal-to-noise ratio of ~39 was calculated, which yielded a 1σ minimum detection limit (MDL) of 5 ppbv for an acquisition time of 1 s. For the selected SO_2 absorption band centered at 1380.93 cm^{-1}, the measured optical power emitted by the QCL was ~203 mW (T = 279.15 K, I = 398 mA). The QCL beam was focused into the gap formed by the two interferometer mirrors with a transmission efficiency of >99.8%. Taking the absorption of the plano-convex lens and the optical window of the gas cell into account, an optical power of ~174 mW was directed through the two mirrors to interact with the sample gas. The normalized noise equivalent absorption (NNEA) coefficient at unit laser power and at unit bandwidth, which allows a comparison of indirect spectroscopic sensors, was calculated to be NNEA = 7.5×10^{-9} cm^{-1} W $Hz^{-1/2}$, using a minimum detectable SO_2 absorption coefficient of $\alpha_{min} = 1.32 \times 10^{-8}$ cm^{-1}, an optical excitation power of $P = 174$ mW, and a detector bandwidth of $\Delta f = 94$ mHz ($\tau = 1$ s, 18 dB/oct low-pass filter).

Optics EXPRESS

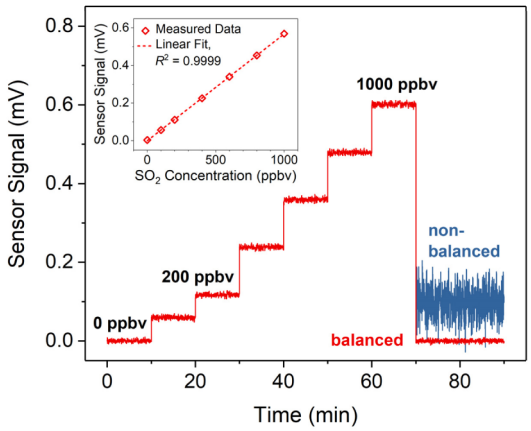

Fig. 6. Stepwise measurement of different SO_2 concentration levels, as well as the sensor noise for balanced and non-balanced ICAPS detection; inset: linear sensor response of measured signal amplitudes versus SO_2 gas concentration.

The system's shot noise level for the basic balanced detection setup composed of the two photodetectors and the 50:50 split NIR fiber laser output, but without transmission through the cavities, was determined by recording noise power spectra with a spectrum analyzer. To ensure that the same power was impinging on the detectors as for the case of transmission through the cavities, the beams were attenuated by additional neutral density filters, accounting for any power losses, which are caused by transmission through the cavities. By this means, the shot noise level of the laser – photodetectors system could be determined [15], excluding any potential noise contribution by the cavities. Here, the measured difference between the noise power levels for balanced and non-balanced detection around the second harmonic of the f_{mod} yielded an improvement by 24.1 dB by canceling the probe laser excess noise. This result is in very good agreement with the measured improvement of 21.1 dB for the standard deviation of the noise using balanced-detection ICAPS, indicating sensor operation only 3 dB (factor 1.4) above the determined shot noise level. The small discrepancy from optimum noise canceling performance of balanced-detection ICAPS may be caused by a little imbalance of the two detector channels.

3.3. Long-term stability

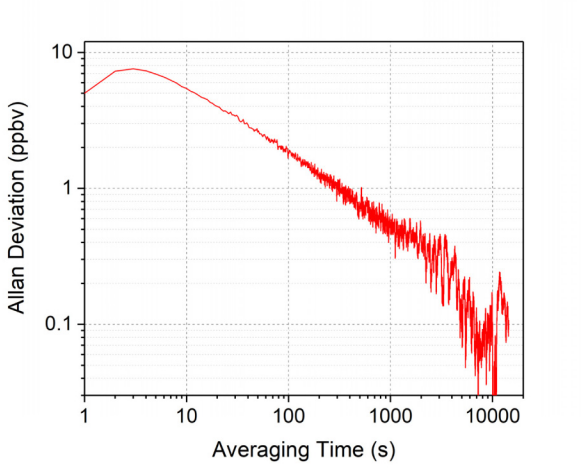

Fig. 7. Allan-Werle deviation plot for measurement of pure N_2 over 8 h.

Optics EXPRESS

To investigate the long-term stability and noise characteristics of the balanced-detection ICAPS scheme, an Allan-Werle variance analysis [21] was performed. For this purpose, pure N_2 was passed through the sensor while the QCL was locked to the SO_2 absorption line. Data were recorded for a total duration of 8 h. The Allan deviation shown in Fig. 7 indicates excellent stability of the sensor. The balanced-detection ICAPS scheme is dominated by white noise characteristics that do not show any additional sensor drift up to an average time of a few 1000 s due to inherent compensation of slow drifts by this technique. This white-noise-dominated region allows for long-duration signal averaging, which proportionally improves the sensitivity. For example, a 10-fold improvement in sensitivity, i.e., a MDL of approximately 500 pptv SO_2, can be estimated using an integration time of 1000 s. The initial increase in the Allan plot up to an average time of approximately 3 s indicates a typical low-pass filter characteristic [22], which is due to the employed LIA settings (Δf = 94 mHz, 18 dB/oct low-pass filter).

4. Conclusions and outlook

The work presented herein illustrates highly sensitive and selective trace-gas sensing by the newly developed balanced-detection ICAPS method; the capabilities of the method were demonstrated on the example of SO_2 detection down to the single digit ppbv concentration range by employing a mid-infrared CW-DFB-QCL as the excitation source. The use of a Fabry-Perot interferometer as transducer for the photo-induced changes in the refractive index has the unique ability to additionally adjust the sensitivity, i.e., the slope of the transmission function, via the finesse of the cavity, facilitating miniaturization of the sensitive sensor. The miniaturization of highly sensitive gas detectors is of big request among different fields due to specific characteristics such as the small absorption volume or simply the small footprint, but remains challenging. The more established methods based on direct absorption spectroscopy only show a limited potential for sensor miniaturization due to their dependence of the sensitivity on the optical path length according to the Lambert-Beer law. A small absorption volume may be of interest for detection of rapidly changing concentration levels in gas streams due to the capacity for rapid sample gas exchange, or for applications where only limited sample gas volumes are available. A potential drawback of the PTI technique is its susceptibility to specific noise sources, such as transducer noise and environmental noise, which contribute to the measured analytical signal. To compensate for this drawback and unleash the full potential of the technique, additional noise reduction strategies are needed when aiming for robust implementations. By application of two identical cavities, balanced-detection ICAPS combines the advantages of conventional PTI, employing a single Fabry-Perot interferometer as transducer, together with enhanced sensitivity and ruggedness, which result from the balanced-detection scheme. The balanced-detection scheme is a key tool for improving the sensitivity of ICAPS-based sensors due to its effective rejection of common mode noise down to the limit of shot noise, thereby preventing any proportional increase in the noise with increasing cavity finesse. The data presented here clearly indicate the excellent ability of the described balanced-detection scheme to significantly improve the analytical figures of merit of a Fabry-Perot interferometer-based photothermal gas sensor. This is demonstrated by achieving a sensor noise floor of only 3 dB (factor 1.4) above the shot noise level. The achieved MDL of 5 ppbv SO_2 and the corresponding NNEA of 7.5×10^{-9} cm^{-1} W Hz$^{-1/2}$ improves upon a previous QCL-based ICAPS sensor for SO_2 detection [14] by a factor of 240 in terms of sensitivity as expressed via NNEA due to various applied measures, including reduced sensor noise level and enhanced transducer signal. Furthermore, the presented sensor outperforms a comparable photoacoustic sensor for SO_2 detection [23] by a factor of 149, again comparing sensitivity as expressed via the NNEA value. The absence of any resonance allows the free selection of the modulation (detection) frequency. Because PTS signals are inversely proportional to the modulation frequency, this characteristic allows selection of the optimum modulation frequency in terms of the

Optics EXPRESS

maximum ratio of the photo-induced signal strength versus noise. This feature sets balanced-detection ICAPS apart from most photoacoustic sensors, which use acoustic resonators to improve the induced signal. The use of such resonators with dimensions of a few millimeters to centimeters in length handicaps sensor miniaturization, and because the resonance frequency of these resonators changes with changing environmental conditions, photoacoustic spectroscopy requires frequent recalibration for stable long-term operation. The balanced-detection ICAPS scheme exhibited white-noise-determined characteristics, thereby resulting in excellent long-term stability due to feedback-controlled compensation of transducer drifts, which additionally allows to improve sensitivity by application of integration times of more than a few thousand seconds. This may be of special interest for applications where the concentration of the target molecule either does not change or changes only very slowly. Selectivity of the sensor was achieved by employing the 2*f*-WM method at reduced pressure. A further interesting aspect worth discussing relates to the inherent flexibility of this concept. Because the ICAPS technique is based on indirect detection, it is able to detect any modulated changes of the refractive index of the sample. As such, this method is not limited to a particular excitation wavelength range; it can be applied to a broad range of excitation sources ranging from the UV to the THz spectral region. In this work, a cavity spacing of 1 mm with a finesse of 89 has been used to detect photothermal signals, which were induced via high laser intensity. The use of higher finesse cavities and higher laser intensities will further improve the sensitivities of the balanced-detection ICAPS sensor system. The presented sensor is based on a simple, compact, and robust arrangement that already has a small detection volume of less than 2 cm^3. In this work, no efforts were made to achieve a smaller gas volume. However, if desired, the volume could easily be reduced, e.g., by application of more compact interferometer substrate dimensions. Such an overall small size and high potential for further miniaturization may be advantageous for certain implementations, such as mobile applications. Considering the required components for a balanced-detection ICAPS system, miniaturization of the system even down to integration on a chip appears to be feasible.

Funding

Austrian Science Fund (PIR 40-N34).

References

1. U. Willer, M. Saraji, A. Khorsandi, P. Geiser, and W. Schade, "Near- and mid-infrared laser monitoring of industrial processes, environment and security applications," Opt. Lasers Eng. **44**(7), 699–710 (2006).
2. H. Moser, W. Pölz, J. P. Waclawek, J. Ofner, and B. Lendl, "Implementation of a quantum cascade laser-based gas sensor prototype for sub-ppmv H_2S measurements in a petrochemical process gas stream," Anal. Bioanal. Chem. **409**(3), 729–739 (2017).
3. A. Amann, W. Miekisch, J. Schubert, B. Buszewski, T. Ligor, T. Jezierski, J. Pleil, and T. Risby, "Analysis of exhaled breath for disease detection," Annu. Rev. Anal. Chem. (Palo Alto, Calif.) **7**(1), 455–482 (2014).
4. J. Hodgkinson and R. P. Tatam, "Optical gas sensing: a review," Meas. Sci. Technol. **24**(1), 012004 (2013).
5. S. E. Bialkowski, *Photothermal Spectroscopy Methods for Chemical Analysis* (John Wiley & Sons, 1996).
6. A. Miklós, P. Hess, and Z. Bozóki, "Application of acoustic resonators in photoacoustic trace gas analysis and metrology," Rev. Sci. Instrum. **72**(4), 1937–1955 (2001).
7. C. C. Davis and S. J. Petuchowski, "Phase fluctuation optical heterodyne spectroscopy of gases," Appl. Opt. **20**(14), 2539–2554 (1981).
8. W. Jin, Y. Cao, F. Yang, and H. L. Ho, "Ultra-sensitive all-fibre photothermal spectroscopy with large dynamic range," Nat. Commun. **6**(1), 6767 (2015).
9. Z. Li, Z. Wang, F. Yang, W. Jin, and W. Ren, "Mid-infrared fiber-optic photothermal interferometry," Opt. Lett. **42**(18), 3718–3721 (2017).
10. D. L. Mazzoni and C. C. Davis, "Trace detection of hydrazines by optical homodyne interferometry," Appl. Opt. **30**(7), 756–764 (1991).
11. A. J. Campillo, S. J. Petuchowski, C. C. Davis, and H.-B. Lin, "Fabry-Perot photothermal trace detection," Appl. Phys. Lett. **41**(4), 327–329 (1982).
12. B. C. Yip and E. S. Yeung, "Wavelength modulated Fabry-Perot interferometry for quantitation of trace gas components," Anal. Chim. Acta **169**, 385–389 (1985).

Optics EXPRESS

13. F. Yang, Y. Tan, W. Jin, Y. Lin, Y. Qi, and H. L. Ho, "Hollow-core fiber Fabry-Perot photothermal gas sensor," Opt. Lett. **41**(13), 3025–3028 (2016).
14. J. P. Waclawek, V. C. Bauer, H. Moser, and B. Lendl, "2f-wavelength modulation Fabry-Perot photothermal interferometry," Opt. Express **24**(25), 28958–28967 (2016).
15. M. Fox, *Quantum Optics: An Introduction* (OUP Oxford, 2006), Chap. 2.
16. P. C. D. Hobbs, "Ultrasensitive laser measurements without tears," Appl. Opt. **36**(4), 903–920 (1997).
17. G. Durry, I. Pouchet, N. Amarouche, T. Danguy, and G. Megie, "Shot-noise-limited dual-beam detector for atmospheric trace-gas monitoring with near-infrared diode lasers," Appl. Opt. **39**(30), 5609–5619 (2000).
18. P. Werle, "A review of recent advantages in semiconductor laser based gas monitors," Spectrochim. Acta A **54**(2), 197–236 (1998).
19. G. A. Reider, *Photonics – An Introduction* (Springer, 2016), Chap. 4.
20. I. E. Gordon, L. S. Rothman, C. Hill, R. V. Kochanov, Y. Tan, P. F. Bernath, M. Birk, V. Boudon, A. Campargue, K. V. Chance, B. J. Drouin, J.-M. Flaud, R. R. Gamache, J. T. Hodges, D. Jacquemart, V. I. Perevalov, A. Perrin, K. P. Shine, M.-A. H. Smith, J. Tennyson, G. C. Toon, H. Tran, V. G. Tyuterev, A. Barbe, A. G. Császár, V. M. Devi, T. Furtenbacher, J. J. Harrison, J.-M. Hartmann, A. Jolly, T. J. Johnson, T. Karman, I. Kleiner, A. A. Kyuberis, J. Loos, O. M. Lyulin, S. T. Massie, S. N. Mikhailenko, N. Moazzen-Ahmadi, H. S. P. Müller, O. V. Naumenko, A. V. Nikitin, O. L. Polyansky, M. Rey, M. Rotger, S. W. Sharpe, K. Sung, E. Starikova, S. A. Tashkun, J. V. Auwera, G. Wagner, J. Wilzewski, P. Wcisło, S. Yu, and E. J. Zak, "The HITRAN2016 molecular spectroscopic database," J. Quant. Spectrosc. Radiat. Transf. **203**, 3–69 (2017).
21. P. W. Werle, P. Mazzinghi, F. D'Amato, M. De Rosa, K. Maurer, and F. Slemr, "Signal processing and calibration procedures for in situ diode-laser absorption spectroscopy," Spectrochim. Acta A Mol. Biomol. Spectrosc. **60**(8-9), 1685–1705 (2004).
22. P. Werle, "Accuracy and precision of laser spectrometers for trace gas sensing in the presence of optical fringes and atmospheric turbulence," Appl. Phys. B **102**(2), 313–329 (2011).
23. J. P. Waclawek, R. Lewicki, H. Moser, M. Brandstetter, F. K. Tittel, and B. Lendl, "Quartz-enhanced photoacoustic spectroscopy-based sensor system for sulfur dioxide detection using a CW DFB-QCL," Appl. Phys. B **117**(1), 113–120 (2014).